In: Arsenic
Editor: Andrea Masotti
ISBN: 978-1-62081-320-1

Chapter 2

ARSENIC SPECIATION IN ROCK-FORMING MINERALS DETERMINED BY EPR SPECTROSCOPY

Yuanming Pan*
Department of Geological Sciences, University of Saskatchewan,
Saskatoon, Canada

ABSTRACT

The mobility, bioavailability and toxicity of arsenic in aqueous environments depend upon its physical distribution and chemical speciation in the source rocks and soils. In this context, enormous efforts have been devoted to investigate arsenic speciation in arsenic-rich minerals, such as sulfarsenides, arsenites, arsenates and sulfides. Most rock-forming minerals (especially silicates), on the other hand, were thought to contain negligible amounts of arsenic and, consequently, were generally ignored with respect to their roles in arsenic contamination and potential applications for remediation, except that clay minerals and zeolites have been investigated for their surface sorption properties. This contribution reviews the present status of EPR-based understanding of arsenic speciation in rock-forming minerals (i.e., carbonates, silicates, phosphates, sulfates and borates) and demonstrates its advantages (e.g., superior sensitivity and unambiguous distinction between lattice-bound and surface-sorpted arsenic species) over other state-of-the-art structural techniques such as synchrotron X-ray absorption spectroscopy. In particular, identification of four arsenic-centered oxyradicals and discussion about the oxidation states, site assignments, local structural environments and substitution mechanisms of their diamagnetic precursors, in selected rock-forming minerals are presented.

INTRODUCTION

Arsenic, usually a trace element in the natural environment, is known to occur in multiple oxidation states from −3 to −1, 0, +3 and +5. The mobility, bioavailability and toxicity of

* Tel: (306) 966-5699, Fax: (306) 966-8593, email: yuanming.pan@usask.ca

arsenic in the environment are known to depend upon its speciation. Therefore, ability to determine arsenic speciation in various hosts at dilute concentrations is important to understanding, management and remediation of arsenic contamination in the environment.

Structural techniques that are commonly used to determine arsenic speciation in minerals and other solids include X-ray and neutron diffraction analyses, synchrotron X-ray absorption spectroscopy, Raman spectroscopy, and nuclear magnetic resonance spectroscopy. However, most of these structural techniques are applicable to arsenic-rich materials only. The arsenic contents in most rock-forming minerals, on the other hand, are usually below 10 ppm [1] and therefore present a major challenge to most structural techniques, including the highly sensitive synchrotron X-ray absorption spectroscopy. In this regard, electron paramagnetic resonance (EPR) spectroscopy that measures interactions between unpaired electrons and electromagnetic radiation is unique, because of its unparallel sensitivity for structural studies of paramagnetic centers at concentrations as low as $\sim 10^{11}$ spins or sub-ppm level [2, 3]. Conventional EPR experiments are done using a constant microwave frequency and scanning the externally applied magnetic field over a suitable range, while maintaining a continuous microwave power incident on the sample (hence known as continuous-wave or CW-EPR). In addition, several related techniques such as electron nuclear double resonance (ENDOR) and electron spin echo envelope modulation (ESEEM) spectroscopy provide structural information about paramagnetic centers containing nuclei with non-zero nuclear spins. Unlike the CW techniques, however, modern ENDOR and ESEEM experiments are commonly made by use of various radiofrequency pulses to excite electron spins [4]. This contribution presents a review of arsenic speciation in rock-forming minerals as determined by those EPR techniques, in comparison with, where available, data from other structural techniques such as synchrotron X-ray absorption spectroscopy.

PARAMAGNETIC ARSENIC-CENTERED RADICALS

There are a large number of organic and inorganic arsenic species with diverse geometric configurations [5], but none of them is intrinsically paramagnetic. Therefore, detection of arsenic by the EPR techniques requires transformation of these diamagnetic species to paramagnetic centers, which can be accomplished by a wide variety of physico-chemical methods such as photolysis and radiolysis. For example, irradiation using X-ray, gamma-ray, electrons or neutrons is commonly applied for converting diamagnetic ions and molecules to paramagnetic centers for EPR studies. On the other hand, arsenic species, when paramagnetic, can often be unambiguously identified by EPR, because of their diagnostic ^{75}As hyperfine structures arising from interaction with the ^{75}As nucleus with the nuclear spin number I =3/2 and natural isotope abundance of 100%. Also, ^{75}As, unlike other I=3/2 nuclei such as ^{11}B and ^{23}Na, is known for its considerable nuclear quadrupole effect [3, 6], which is potentially helpful for identifying arsenic-related paramagnetic species as well.

To date, four arsenic-centered oxyradicals: $[AsO_4]^{2-}$, $[AsO_4]^{4-}$, $[AsO_3]^{2-}$ and $[AsO_2]^{2-}$ have been documented in minerals ([6-17]; Table 1), although numerous organic radicals containing arsenic are known [18, 19]. Of these, the first one is the only hole-like center with $g_{avg} > g_e = 2.0023$, whereas the remaining three are all electron-like centers (Table 1).

Table 1. Spin Hamiltonian parameters of four arsenic-centered oxyradicals in crystalline hosts

Host	g_1	g_2	g_3	A_1/h (MHz)	A_2/h (MHz)	A_3/h (MHz)	Unpaired spin (%)			Ref.
							4s	$4p_z$	$4p_x$	
$[AsO_4]^{2-}$										
Scheelite (77K)	2.0470	2.0122	2.00070	64.4	53.2	52.4	0.39	1.0		7
$(NH_4)_2HPO_4$	2.030(5)	2.023(5)	2.016(5)	87(3)	48(3)	20(3)	0.35	3.3		8
Hemimorphite	2.02407(1)	2.00982(1)	2.00326(1)	60.48(3)	52.15(3)	47.02(3)	0.36	0.7		6
$[AsO_4]^{4-}$										
KDA(4.2K)	2.011(5)	1.995(5)	2.000(4)	3199(2)	2895(3)	2833(3)	20.3	36.6	6.2	9
KDA(296K)	2.001(5)	2.000(5)	2.004(5)	3253(2)	2926(3)	2922(3)	20.7	32.9		9
ADA (296K)	2.006(5)	1.993(5)	1.998(4)	3247(3)	2943(5)	2890(5)	20.7	35.7	5.3	9
RDA(296K)	1.998(4)	1.998(4)	1.998(4)	3183(3)	2870(4)	2867(4)	20.3	31.4		9
CDA(296K)	1.996(5)	1.996(5)	1.996(5)	3115(3)	2805(4)	2805(4)	19.8	31.0		9
Hemimorphite	2.00490(4)	2.00130(4)	1.99568(4)	3683.3(3)	3415.7(3)	3362.1(3)	23.8	32.1	5.4	6
$[AsO_3]^{2-}$										
Calcite (77K)	2.00162(5)	2.00195(5)	2.00195(5)	2626.7(1)	2108.8(2)	2108.8(2)	15.6	51.8		10
$Na_2HAsO_4.7H_2O$	2.004(2)	2.005(2)	2.005(2)	2033(2)	1590(2)	1590(2)	11.9	44.3		11
KH_2AsO_4 (K)	1.996(5)	1.996(5)	1.996(5)	2573	2102	2079	15.4	49.3	2.1	9
KH_2AsO_4 (L)	1.999(5)	1.999(5)	1.999(5)	2145	1704	1693	12.6	45.1	0.9	9
KH_2AsO_4 (M)	2.000(5)	2.000(5)	2.000(5)	1852	1401	1391	10.6	46.0	0.9	9
Struvite (I)	2.0064(2)	2.0085(2)	2.0058(2)	1694(6)	1523(6)	1378(6)	10.4	31.4	14.7	12
Struvite (II)	2.0070(2)	2.0076(2)	2.0058(2)	1697(6)	1525(6)	1366(6)	10.4	33.0	15.9	12
betaine arsenate	2.001(4)	1.998(4)	1.998(4)	1848(10)	1447(10)	1447(10)	10.8	40.1		13
Haidingerite(I)	1.999	1.999	1.999	2388	1885	1885	13.9	53.2		14
Haidingerite(II)	1.998	1.993	1.993	2635	2120	2120	15.6	51.6		14
Gypsum	2.00537(4)	2.00371(5)	2.00134(3)	1952.0(2)	1492.6(2)	1488.7(2)	11.2	46.2		15
$[AsO_2]^{2-}$										
Calcite (4.2K)	2.0150(2)	1.9991(1)	1.9910(2)	614(1)	–152(2)	–173(2)	0.6	78.5	2.1	16
$C_2H_6AsNaO_2$	2.012	1.995	1.967	513	–210	–238	0.1	75.0	3.0	17
Gypsum	2.01484(2)	1.99962(2)	1.9958(1)	475.5(2)	–211.1(2)	–229.5(5)	0.1	70.5	1.8	15

KDA, ADA, RDA and CDA denote KH_2AsO_4, $NH_4H_2AsO_4$, RbH_2AsO_4, and CsH_2AsO_4, respectively. The distribution of unpaired spins in the 4*s* and 4*p* orbitals of arsenic has been re-calculated to the a_0 and b_0 values of 14660 and 333 MHz, respectively (Weil and Bolton 2007).

However, several of the electron-like $[AsO_4]^{2-}$, $[AsO_3]^{2-}$, and $[AsO_2]^{2-}$ radicals in Table 1 have one, two or all three principle g values >2.0023. This is attributable to the spin-orbit coupling expected for As, although analytical uncertainty arising from difficulty in the calibration of the magnetic field for these radicals with large hyperfine structures may be a contributing factor as well. Another arsenic-centered oxyradical $[AsO_2]^0$, which was established in the X-ray-irradiated neon matrix [20], has not been documented in minerals and will not be considered further here. Similarly, other inorganic radicals involving As such as AsF_3^-, $AsCl_3^-$, and AsH_3F [21] are unlikely to be important in rock-forming minerals and are not considered either.

The $[AsO_4]^{2-}$ radical, which was first discovered in gamma-ray-irradiated scheelite $CaWO_4$ [7], is isoelectronic with $[PO_4]^{2-}$, $[SO_4]^-$ and $[SeO_4]^-$[22] and is characterized by trapping of the unpaired electron largely on one of the four oxygen atoms, hence a variety of the classic O^- centers [6, 23, 24]. Its ^{75}As hyperfine coupling constants, with a principle $A(^{75}As)$ axis along one As−O bond direction, are expected to be small (Table 1) and arise from spin polarization [8,24]. In scheelite the precursor $[AsO_4]^{3-}$ relative to the host $[WO_4]^{2-}$ contains one excess electron and therefore is an ideal candidate for losing an electron to form the $[AsO_4]^{2-}$ radical during radiolysis [7]:

$$[AsO_4]^{3-} - e \rightarrow [AsO_4]^{2-} \quad (1)$$

The $[AsO_4]^{4-}$ radical, isoelectronic with PF_4, $[PO_4]^{4-}$, $[SeO_4]^{3-}$ and $[SO_4]^{3-}$, was first identified by Hampton et al. [25] in X-ray-irradiated KH_2AsO_4 (KDA) at room temperature. Similar to the $[AsO_4]^{2-}$ radical, the diamagnetic precursor for the $[AsO_4]^{4-}$ radical is undoubtedly the $[AsO_4]^{3-}$ group as well [9, 25-27]:

$$[AsO_4]^{3-} + e \rightarrow [AsO_4]^{4-} \quad (2)$$

Here, the $[AsO_4]^{3-}$ precursor in arsenates and phosphates has all the valence shells of the oxygen atoms fully filled, so that the additional electron trapped during irradiation can be accommodated only by the central arsenic via a steric transformation involving its 4*d* orbital [27]. Therefore, sp^3 hybridization results in significant amounts of the unpaired spin on the 4*s* and 4*p* orbitals, yielding large ^{75}As hyperfine coupling constants (Table 1).

The $[AsO_3]^{2-}$ radical, isoelectronic with $[PO_3]^{2-}$, $[NO_3]^{2-}$, $[SO_3]^-$, $[SeO_3]^-$ and ClO_3[22], was first identified in X-ray-irradiated Na_2HAsO_4[11]. This radical has a pyramidal structure involving *sp3* hybridization with large amounts of the unpaired spin on the *4s* and *4p* orbitals of the arsenic atom, hence its large ^{75}As hyperfine coupling constants. However, the ^{75}As hyperfine coupling constants of the $[AsO_3]^{2-}$ radical are notably smaller than those of the $[AsO_4]^{4-}$ center (Table 1). Moreover, the spin-density ratios between the 4*s* and 4*p* orbitals of the $[AsO_3]^{2-}$ radical are significantly smaller than those of the $[AsO_4]^{4-}$ center (Table 1). In gamma-ray irradiated haidingerite ($CaHAsO_4 \cdot H_2O$), Gilinskaya and Afanas'eva [12] observed two varieties of the $[AsO_3]^{2-}$ radical and suggested the following radio-chemical reaction for their formation:

$$[HAsO_4]^{2-} - e \rightarrow [AsO_3]^{2-} + OH^- \quad (3)$$

The $[AsO_2]^{2-}$ radical is isostructural with the ClO_2, NO_2^{2-} and SeO_2^{-} centers [16] and has an approximately planar configuration with sp^2 hybridization, resulting in almost all the unpaired electron localized on the *4p* orbital of arsenic (Table 1). The $[AsO_2]^{2-}$ radical, unlike the $[AsO_4]^{2-}$, $[AsO_4]^{4-}$ and $[AsO_3]^{2-}$ radicals from the $[AsO_4]^{3-}$ precursor, apparently forms from the $[AsO_3]^{3-}$ group via a reaction of the type:

$$[AsO_3]^{3-} - O^{2-} + e \rightarrow [AsO_2]^{2-} \quad (4)$$

Therefore, four types of arsenic-centered oxyradicals are readily distinguishable on the basis of their characteristic ^{75}As hyperfine coupling constants, although small variations within each type are present (Table 1) and are probably attributable to the crystal field effects. The ^{75}As hyperfine coupling constants of these radicals are all consistent with the expectations of their respective electronic structures. Also, Reactions 1-4 show that the diamagnetic precursors to these arsenic-centered oxyradicals are all known. Therefore, their EPR detection immediately provides detailed information about arsenic such as its oxidation state, coordination number, and the next-nearest nuclei if superhyperfine structure(s) are observed. Spin Hamiltonian parameters from single-crystal EPR studies also provide additional information about site assignments and formation mechanisms of individual arsenic-centered oxyradicals in minerals investigated.

CARBONATES

The presence of elevated arsenic contents in natural calcite ($CaCO_3$) has attracted numerous recent studies using a variety of the state-of-the-art structural techniques and sophisticated first-principles calculations to investigate the roles and applications of this mineral for remediation of arsenic contamination in the environment [28-35]. These studies have provided compelling evidence for the incorporation of both ^{V}As and ^{III}As at the carbon site in calcite. In this regard, it is surprising that these recent studies appeared to have overlooked the fact that CW-EPR studies of Serway and Marshall [10] and Marshall and Serway [16] established lattice-bounded As(V) and As(III) at the carbon site in natural calcite some 40 years ago.

Serway and Marshall [10], in their single-crystal EPR study of gamma-ray-irradiated calcite containing 1 to 40 ppm As, observed an axially symmetrical center characterized by a four-component hyperfine structure. They noted that the symmetry axis of this center coincides with the crystal c-axis direction and reported its spin Hamiltonian parameters at 77 K (Table 1), including the nuclear quadrupole coupling constant $e^2qQ = -2.4$ MHz. These results allowed Serway and Marshall [10] to interpret this center to be the AsO_3^{2-} radical as a substitution for the CO_3^{2-} group in the calcite lattice. Serway and Marshall [10] noted that this radical is not detectable in crystals that were irradiated and measured at 77 K but is observed after the samples have been warmed to room temperature or by performing irradiation at room temperature. Also, the growth of the AsO_3^{2-} radical at room temperature in crystals irradiated at 77 K is accompanied by the simultaneous decay of the CO_3^{3-} center. These results led Serway and Marshall [32] to suggest that the AsO_3^{2-} radical in calcite is not a primary radiation product but probably formed from charge trapping.

Marshall and Serway [6] observed the AsO_2^{2-} radical in single-crystal EPR spectra of the same suite of gamma-ray-irradiated calcite, measured at 4.2 K. The g and A(^{75}As) matrices of this radical are approximately axial in symmetry and have their unique principle axes along the crystal c-axis direction and a C−O bond direction, respectively, confirming its location at the carbonate ion site. All spin Hamiltonian parameters of this radical, including the nuclear quadrupole coupling constant e^2qQ = 16.2 MHz and the asymmetric parameter $\eta \cong 0$, are consistent with the AsO_2^{2-} model with a planar configuration involving sp^2 hybridization and the unpaired electron largely localized in the 4*p* orbital of the arsenic atom.

Di Benedetto et al. [30] measured ESEEM spectra for Mn- and As-bearing calcite (i.e., travertine) in both the field-domain and time-domain (two-pulse Hahn echo, 2p) modes, at temperature of 4.2 K and operating frequency of 9.717 GHz. Their two-pulse ESEEM spectra revealed superimposed nuclear modulations, which have been shown by spectral simulations to arise from the presence of ^{75}As at the carbon site with a Mn-As distance comparable to the Ca-C distance in calcite [32]. Di Benedetto et al. [30] suggested a substitution of $[AsO_3]^{3-} \rightarrow [CO_3]^{2-}$ for incorporating arsenic in calcite, and their confirmation of As(V) came from a subsequent synchrotron X-ray absorption spectroscopic study [31].

SILICATES

Rock-forming silicates were thought to contain ≤3 ppm As [1], although rare arsenosilicates such as ardennite, mediate and tiragalloite are known but do not involve any isomorphous substitution between As and Si[36,37]. Direct evidence of isomorphous substitutions between $[^{V}AsO_4]^{3-}$ and $[SiO_4]^{2-}$ in silicates has been documented only recently. For example, Vergasova et al. [38] and Filatov et al. [39] reported filatovite $K[(Al,Zn)_2(As,Si)_2O_8]$, which is the first arsenate of the feldspar group and involves the coupled substitution $Zn^{2+} + As^{5+} = Al^{3+} + Si^{4+}$, from the Tolbachik volcano, Kamchatka peninsula, Russia. Charnock et al. [40] reported data from synchrotron As K-edge X-ray absorption spectra for the substitution of As^{5+} for Si^{4+} in garnet containing 2,500 ppm As, from the Central Oslo Rift. Interestingly, the synchrotron X-ray absorption spectroscopic studies of Hattori et al. [41] and Pascua et al. [42] documented elevated As contents, including the identification of As^{5+}, in smectite and antigorite but were unable to determine whether arsenic in these cases represents isomorphous substitution for Si, surface absorption or contamination from impurity phases.

Single-crystal EPR measurements by Mao et al. [6] revealed the presence of the $[AsO_4]^{4-}$ and $[AsO_4]^{2-}$ radicals with characteristic ^{75}As hyperfine structures (Fig. 2a) in a suite of gamma-ray-irradiated hemimorphite ($Zn_4(Si_2O_7)(OH)_2 \bullet H_2O$) from various Zn-Pb-Cu-Ag-Au deposits. Mao et al. [6] noted that the half lifes of the $[AsO_4]^{4-}$ and $[AsO_4]^{2-}$ radicals are 21 and 29 days, respectively. Each hyperfine component of the $[AsO_4]^{4-}$ radical in the single-crystal EPR spectra is resolved into four lines when the magnetic field is rotated away from crystal axes, indicative of a triclinic site symmetry in the orthorhombic hemimorphite. On the other hand, each hyperfine component of the $[AsO_4]^{2-}$ radical is resolved into at most two lines, indicating a monoclinic site symmetry. In addition, spectral simulations confirmed that the weak doublet accompanying each hyperfine component of the $[AsO_4]^{2-}$ radical (Fig. 2b) represents the ^{29}Si superhyperfine structure arising from interaction with a single ^{29}Si nucleus

with I = ½ and natural isotope abundance = 4.7%. Spectral simulations showed that additional weak lines of the $[AsO_4]^{2-}$ radical arise from a considerable nuclear quadrupole effect (Fig. 2b), which is characteristic of the ^{75}As nucleus and thus providing further confirmation for the identification of this arsenic-associated radical. Moreover, each main line of the $[AsO_4]^{2-}$ radical in a few spectra measured at specific crystal orientations is resolved into three components with an intensity ratio of 1:2:1, attributable to ^{1}H superhyperfine structure arising from interaction with two equivalent or nearly equivalent hydrogen nuclei (I=1/2 and isotope abundance = ~100%).

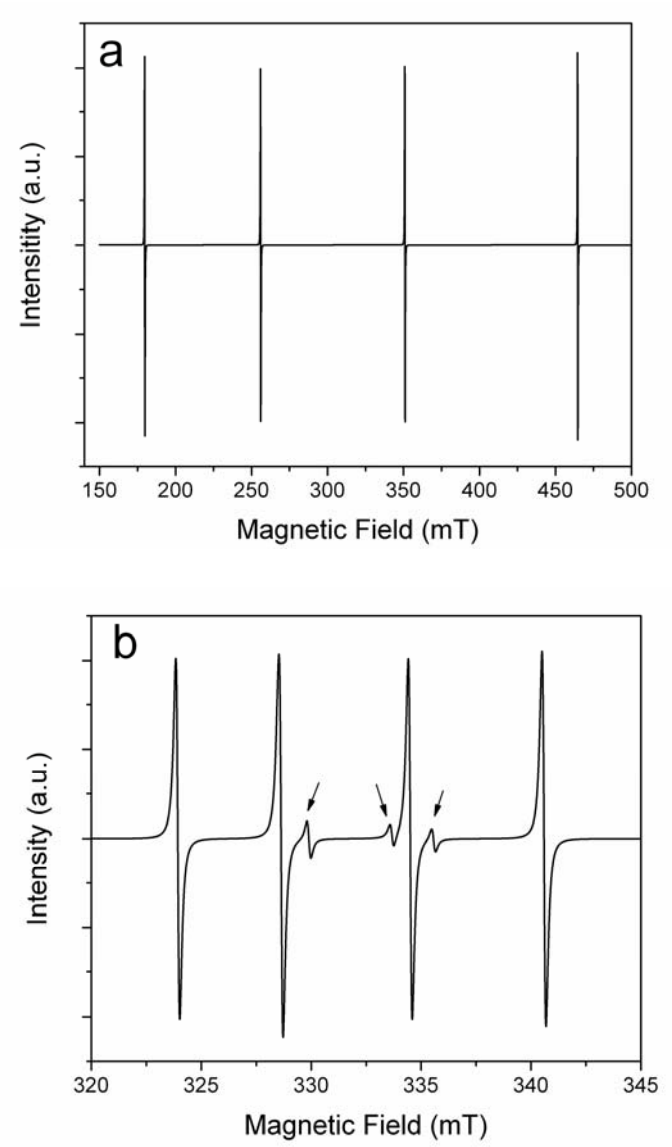

Figure 1. Simulated single-crystal EPR spectra of a) the $[AsO_3]^{2-}$ radical and b) the $[AsO_2]^{2-}$ radical in calcite, with the magnetic field along the crystal c-axis direction and microwave frequency = 9.388 GHz: Note that weak lines marked by arrows in b) arising from the nuclear quadrupole effect (data from [10] and [16]).

The best-fit spin Hamiltonian parameters of the $[AsO_4]^{4-}$ radical have the orientations of the $g_{intermediate}$ and $A_{maximum}$ principle axes both approximately along one of the pseudo-tetrad axes of the SiO_4 tetrahedron in hemimorphite, confirming the location of arsenic at the Si site. Similarly, the best-fit orientations of the $g_{maximum}$ and $A_{maximum}$ principle axes of the $[AsO_4]^{2-}$ radical are close to the Si−O4 bond direction, also confirming the location of this radical at the SiO_4 tetrahedral position and the unpaired electron largely on the non-bonding orbital of the O4 atom. This structural model for the $[AsO_4]^{2-}$ radical is further supported by the observed ^{29}Si and ^{1}H superhyperfine structures (Fig. 2b). For example, the magnitude of ^{29}Si superhyperfine splitting at ~1 mT (Figure 2b) supports the presence of a nearest-neighbor Si atom. Also, the O4 atom has two equivalent hydrogen atoms at ~3.5 Å, which is consistent with the dipole-dipole-model prediction from the observed ^{1}H superhyperfine splitting of ~0.3 mT[6].

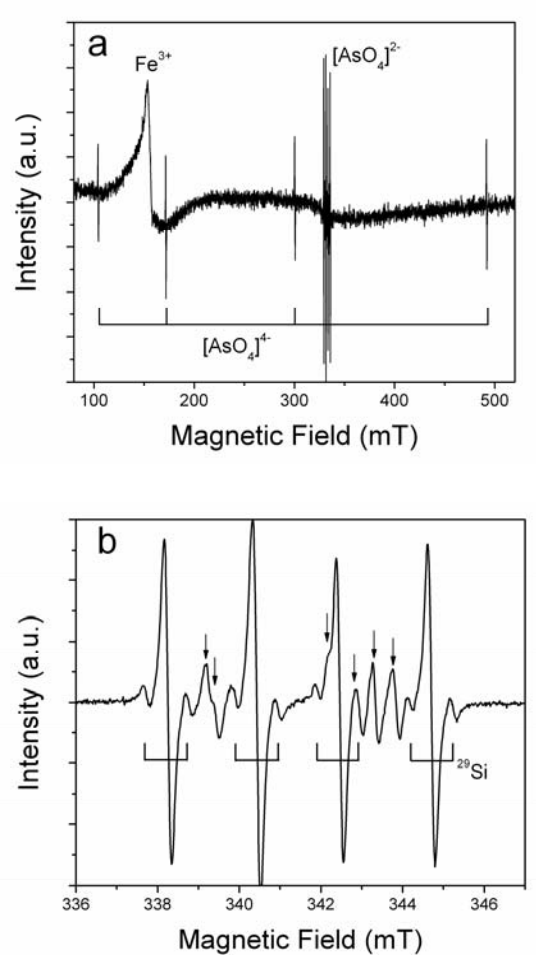

Figure 2. Representative single-crystal EPR spectra of gamma-ray-irradiated hemimorphite with the magnetic field parallel to the crystal c-axis and: a) wide-scan spectrum at a microwave frequency of 9.36 GHz showing the Fe^{3+} center and the $[AsO_4]^{2-}$ and $[AsO_4]^{4-}$ radicals, and b) narrow-scan spectrum at a microwave frequency of 9.61 GHz showing the $[AsO_4]^{2-}$ radical with the ^{29}Si superhyperfine structure and additional weak lines (marked by arrows) arising from the nuclear quadrupole effect (modified from [6]).

Mao et al. [6] interpreted the $[AsO_4]^{2-}$ radical in hemimorphite to originate from a substitutional $[AsO_4]^{3-}$ group at the SiO_4 tetrahedral position without an immediate charge compensator. Such an $[AsO_4]^{3-}$ group in comparison with the $[SiO_4]^{2-}$ group that it replaces for contains one extra electron and therefore is an ideal candidate for trapping an hole to form the $[AsO_4]^{2-}$ radical during gamma-ray irradiation. Similarly, Mao et al. [6] interpreted the $[AsO_4]^{4-}$ radical in hemimorphite to form from a substitutional $[AsO_4]^{3-}$ group at the SiO_4 tetrahedral position as well. However, the $[AsO_4]^{3-}$ precursor for the formation of the $[AsO_4]^{4-}$ radical most likely has a neighboring charge compensator (e.g., Cu^{+} at the Zn^{2+} site), yielding a neutral configuration that is capable for trapping an electron during gamma-ray irradiation.

Interestingly, inductively coupled plasma mass spectrometric (ICPMS) analyses of the hemimorphite samples yielded 6 to 338 ppm As [6]. Powder EPR spectrum of the sample containing only 6 ppm As shows that the $[AsO_4]^{4-}$ radical is readily detectable, whereas the $[AsO_4]^{2-}$ radical is superimposed by other radiation-induced centers in the central magnetic field (Figure 3). Spectral simulations with spin Hamiltonian parameters obtained from the single-crystal EPR study [6] reproduce the powder EPR spectrum of the $[AsO_4]^{4-}$ radical very well (Figure 3).

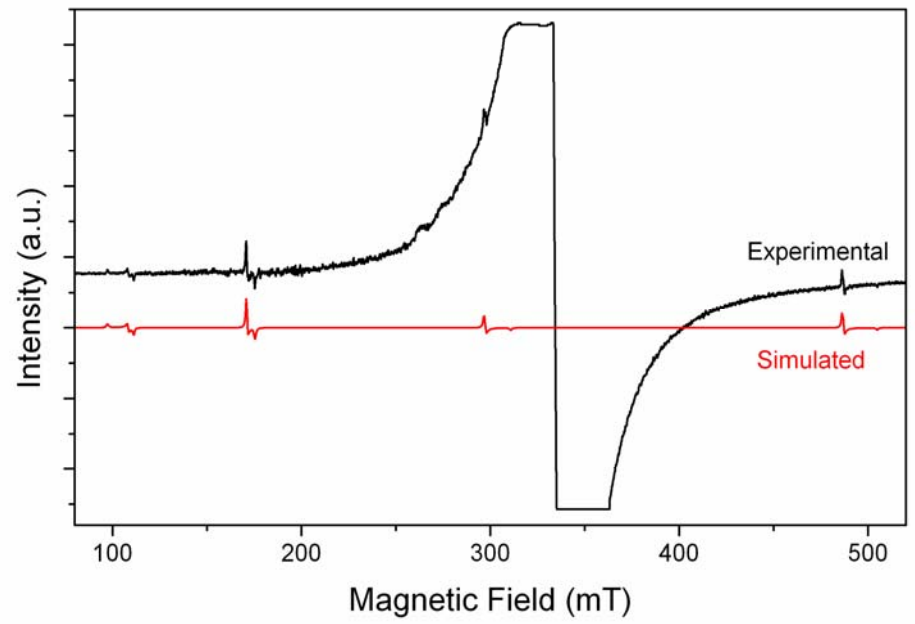

Figure 3. Powder EPR spectrum of a hemimorphite sample containing 6 ppm As measured at ν=9.387 GHz, in comparison with a simulated spectrum using the spin Hamilton parameters of the $[AsO_4]^{4-}$ radical from [6]. Note that the $[AsO_4]^{2-}$ radical in the central region of the magnetic field is not visible owing to the presence of other paramagnetic centers.

PHOSPHATES

Chemical similarities between the arsenate and phosphate groups are well known, and extensive substitutions of $[^{V}AsO_4]^{3-}$ for $[PO_4]^{3-}$ in apatites ($Ca_{10}(PO_4)_6(F,Cl,OH)_2$) and other

phosphates are well documented[43,44]. Table 1 shows that arsenic-centered oxyradicals are well established in phosphates, and EPR studies have identified a variety of paramagnetic radicals such as CO_3^{3-}, CO_3^{-}, SO_3^{-}, SiO_3^{-} and CrO_4^{3-} in the PO_4^{3-} position in apatites [43, 45, 46]. Therefore, it is surprising to note that arsenic-centered oxyradicals have not yet been detected in apatites.

Struvite $(NH_4)Mg(PO_4)•6H_2O$, a major constituent of kidney, bladder and urinary stones in animals and human and an increasingly important fertilizer recovered from sewer and wastewater systems [47,48], is a common mineral in guano and dung deposits, peat beds and organic-rich sediments. Struvite having an arsenate analog $(NH_4)Mg(AsO_4)•6H_2O$ also has been proposed to be useful for the removal of As and other metalloids [49, 50]. Xu [12], on the basis of single-crystal EPR measurements, reported two $[AsO_3]^{2-}$ radicals in gamma-ray-irradiated, arsenate-doped struvite (Table 1). However, careful examination of the descriptions in [12] reveals that they are two magnetically non-equivalent sites of the same $[AsO_3]^{2-}$ radical, rather than two distinct species. Moreover, the EPR spectra reported in [12] appear to include an uncharacterized $[AsO_2]^{2-}$ radical. Therefore, a further EPR study of struvite is warranted to investigate whether this important biomineral is capable of accommodating both As(V) and As(III) in its lattice.

SULFATES

Similarly, the arsenate and sulfate groups share chemical similarities, and extensive substitutions of $[^{V}AsO_4]^{3-}$ for $[SO_4]^{2-}$ have been documented in a number of sulfates such as jarosite [51, 52]. Gypsum ($CaSO_4•2H_2O$), which is the most common sulfate mineral, is a major by-product containing elevated arsenic contents, from the mining and milling processes of borate, phosphate and uranium deposits. For example, production of boric acid from Turkish borate deposits yields an annual output of 2.5 billion tonnes of arsenic-boron-bearing gypsum sludge (also known as "arsenical borogypsum wastes" [53, 54]). Several studies [28, 55-58] investigated incorporation of arsenic in gypsum but reported contradictory results. For example, Rodriguez-Blanco et al. [55], in a SEM-EDS study of co-crystallized pharmacolite ($CaHAsO_4.2H_2O$) and gypsum, did not detect any substitution between As^{5+} and S^{6+}. On the other hand, Fernandez-Martinez et al. [53, 54], in their studies of synthetic gypsum by combined neutron and X-ray diffraction analyses, synchrotron X-ray absorption spectroscopy (XAS) and density functional theory (DFT) modeling, reported substitution of As^{5+} for S^{6+} (see also [28]). This discrepancy most likely stems from different sensitivities of the analytical techniques employed in previous studies [55-58].

Single-crystal EPR studies of gamma-ray-irradiated arsenic-doped gypsum have identified both the $[AsO_3]^{2-}$ and $[AsO_2]^{2-}$ radicals [15]. The $[AsO_3]^{2-}$ center is characterized by its unique A(^{75}As) axis along the S-O1 bond direction, and contains an ^{1}H superhyperfine structure arising from interaction with at least four neighboring protons, which has been confirmed by pulse electron nuclear double resonance (ENDOR) spectra measured at 20 K. These results show that the $[AsO_3]^{2-}$ center formed from electron trapping on the central As^{5+} ion of a substitutional $(AsO_4)^{3-}$ group after removal of an O1 atom. The $[AsO_2]^{2-}$ center is characterized by its unique A(^{75}As) axis approximately perpendicular to the O1-S-O2 plane and the A_2 axis along the S-O2 bond direction, consistent with electron trapping on the central

As^{3+} ion of a substitutional $(AsO_3)^{3-}$ group after removal of an O2 atom [15]. It is also interesting to note that the $[AsO_3]^{2-}$ center predominates over its $[AsO_2]^{2-}$ counterparts in the crystal synthesized with an arsenate in the starting material, but reverse is true in another crystal from an arsenite-bearing starting material. This result supports Reactions 3 and 4 that the $[AsO_3]^{2-}$ and $[AsO_2]^{2-}$ radicals originate from the arsenate and arsenite precursors, respectively. Therefore, this EPR study not only confirms previous suggestions for lattice-bound As^{5+} in gypsum [28, 55, 56], but demonstrates incorporation of As(III) in gypsum as well.

BORATES

The few reported analyses of arsenic in borates were based on bulk-chemical techniques [59] and may not be reliable, because these minerals commonly occur in intimate association with sulfarsenides [60, 61]. Synchrotron micro-X-ray fluorescence mapping and analyses [61] revealed up to 125 ppm As in colemanite ($CaB_3O_4(OH)_3 \bullet H_2O$), a major ore mineral in world-class borate deposits. Modeling of As K-edge X-ray absorption spectra suggests that both As(III) and As(V) are present and preferentially occupy the triangular B1 site and the tetrahedral B2 and site, respectively [61].

Single-crystal EPR spectra of gamma-ray-irradiated colemanite, measured at 40 K, show the presence of an $[AsO_3]^{2-}$ radical with an angular dependence indicative of its accommodation in the crystal lattice [61]. However, quantitative spin Hamiltonian analysis for this radical in colemanite was not possible owing to its spectra having exceedingly low signal-to-noise ratios, even after high doses of gamma-ray irradiation. This example illustrates the limitation of the EPR method in cases where conversion from diamagnetic precursors to paramagnetic centers is inefficient. In such cases, the EPR method would be best combined with synchrotron X-ray absorption spectroscopy, provided that the arsenic contents in the minerals investigated are sufficiently high for the latter technique.

CONCLUSION

In summary, EPR spectroscopy, including related techniques such as pulse ENDOR and ESEEM, is known for its superior sensitivity over other structural techniques and provides a wealth of information about arsenic speciation in rock-forming minerals. In particular, single-crystal EPR studies allow not only unambiguous identification of As^{3+} and As^{5+} but determination of their site assignments and local structural environments in rock-forming minerals.

ACKNOWLEDGMENTS

I would like to thank Mao Mao for provision of the experimental EPR spectrum in Figure 3, and Rong Li, Jinru Lin, Mao Mao and Mark J. Nilges for collaborations on the EPR studies of arsenic in rock-forming minerals.

REFERENCES

[1] P. L. Smedley and D.G. Kinninburg, *Appl. Geochem*. 17, 517 (2002).

[2] Y. Pan, N. Chen, J. A.Weil and M.J. Nilges, *Amer. Mineral*. 87, 1333, (2002).

[3] J. A. Weil and J. R. Bolton *Electron Paramagnetic Resonance: Elementary Theory and Practical Applications.* John Wiley and Sons, New York (2007).

[4] A. Schweiger and G. Jeschke *Principles of Pulse Electron Paramagnetic Resonance*. Oxford University Press, New York (2001).

[5] P. A. O'Day, *Elements* 2, 77 (2006).

[6] M. Mao, J. Lin and Y. Pan, *Geochim. Cosmochim. Acta* 74, 2943 (2010).

[7] P. R. Edwards, S. Subramanian and M. C. R. Symons, *Chem. Commun*. 799 (1968).

[8] S. Subramanian, P. N. Murty, and C. P. K. Murty, *J. Phys. Chem. Solids* 38, 825 (1977).

[9] N. S. Dalal, J. R. Dickson and C. A. McDowell, *J. Chem. Phys*. 57, 4254 (1972).

[10] R. A. Serway and S. A. Marshall, *J. Chem. Phys*. *45*, 2309 (1966).

[11] W. C. Lin and C. A. McDowell, *Mol. Phys*. 7, 223 (1964).

[12] R. Xu, *Phys. Stat. Sol. (b)* 172, K15 (1992).

[13] A. Pöppl, O. Tober and G. Völkel, *Phys. Stat. Sol. (b)* 183, K63 (1994).

[14] L. G. Gilinskaya and V. I. Afanas'eva, *J. Struct. Chem*. 22, 187 (1981).

[15] J. Lin, N. Chen, M. J. Nilges and Y. Pan, (ms)

[16] S. A. Marshall and R. A. Serway, *J. Chem. Phys*. 50, 435 (1969).

[17] M. Geoffroy and A. Llinares, *Helvet. Chim. Acta* 62, 1605 (1979).

[18] E. Furimsky, J. A. Howard and J. R. Morton, *J. Am. Chem. Soc*. 95, 6574 (1973).

[19] M. Geoffroy, A. Llinares and J. R. Morton, *Helv. Chim. Acta* 66, 673 (1983).

[20] L. B. Jr. Knight, G. C. Jones, G. M. King, R. M. Babb and A. J. McKinley, *J. Chem. Phys*. 103, 497 (1995).

[21] A. J. Colussi, J. R. Morton and K. F. Preston, *J. Phys. Chem*. 79, 1855 (1975).

[22] P. W. Atkins and M. C. R. Symmons,*The Structure of Inorganic Radicals: An Application of Electron Spin Resonance to the Study of Molecular Structure*. Elsevier, New York (1967).

[23] O. F. Schirmer, *J. Phys. Conden. Matt*. 18, 667 (2006).

[24] Z. Li and Y. Pan, *Phys. Rev. B* 84, 115112 (2011).

[25] M. Hampton, F. G. Herring, W. C. Lin and C. A. McDowell, *Mol. Phys*. 10, 565 (1966).

[26] N. S. Dalal, J. A. Hebden, D. E. Kennedy and C. A. McDowell, *J. Chem. Phys*. 6, 4425 (1977).

[27] P. N. Murty, C. P. K. Murty and S. Subramanian, *Phys. Stat. Sol. (a)* 39, 675 (1977).

[28] G. Roman-Ross, L. Clarlet, G. J. Cuello and D. Tisserand, *J. Phys. IV France* 107, 1153(2003).

[29] G. Roman-Ross, G. J. Cuello, X. Turrillas, A. Fernandez-Martinez and L. Charlet, *Chem. Geol*. 233, 328 (2006).

[30] F. Di Benedetto, P. Costagliola, M. Benvenuti, P. Lattanzi, M. Romanelli and G. Tanelli, *Earth Planet. Sci. Lett*. 246, 458 (2006).

[31] V. G. Alexandratos, E. J. Elzinga and R. J. Reeder, *Geochim. Cosmochim. Acta* 71, 4172 (2007).

[32] M. Romanelli, M. Benvenuti, P. Costagliola, F. Di Benedetto and P. Lattanzi, *Atti del 1 Meeting SIMP-AIC, Sestri Levante, 7–12 Settembre* (2008).
[33] H. U. Sø, D. Postma, R. Jakobsen and F. Larsen, *Geochim. Cosmochim. Acta* 72, 5871 (2008).
[34] Y. Yokoyama, S. Mitsunobu, K. Tanaka, T. Itai and Y. Takahashi, *Chem. Lett*. 38, 910 (2009).
[35] F. Bardelli, M. Benvenuti M, P. Costagliola, F. Di Benedetto, P. Lattanzi, C. Meneghini, M. Romanelli and L. Valenzano, *Geochim. Cosmochim. Acta* 75, 3011 (2011).
[36] C. M. Gramaccioli, G. Liborio and T. Pilati, *Acta Crystal*. 37, 1972 (1981).
[37] M. Nagashima and T. Armbruster, *Mineral. Mag*. 74, 55 (2010).
[38] L. P. Vergasova, S. V. Krivovichev, S. N. Britvin, P. C. Burns and V. V. Ananiev, *Eur. J. Mineral*. 16, 533 (2004).
[39] S. K. Filatov, S. V. Krivovichev, P. C. Burns and L. P. Vergasova, *Eur. J. Mineral.* 16, 537 (2004).
[40] J. M. Charnock, D. A. Polya, A. G. Gault and R. A. Wogelius, *Amer. Mineral.* 92, 1856 (2007).
[41] K. Hattori, Y. Takahashi, S. Guillot and B. Johanson, *Geochim. Cosmochim. Acta* 69, 5585 (2005).
[42] C. Pascua, J. Charnock, D. A. Polya, T. Sato, S. Yokoyama and M. Minato, *Mineral. Mag*. 69, 897 (2005).
[43] Y. Pan and M. E. Fleet, *Rev. Mineral. Geochem*. 48, 13 (2002).
[44] Y. J. Lee, P. W. Stephens, Y. Tang, W. Li, B. L. Phillips, J. B. Parise and R. J. Reeder, *Amer. Mineral*. 94, 666 (2009).
[45] S. Nokhrin, Y. Pan and M. J. Nilges, *Amer. Mineral*. 91, 1425 (2006).
[46] L. G. Gilinskaya, *Phosphorus, Sulfur, and Silicon and the Related Elements* 51, 438 (2009).
[47] L. Shu, P. Schneider, V. Jegatheesan and J. Johnson, *Biores. Tech*. 97, 2211 (2006).
[48] K. P. Fattah, Y. Zhang, D. S. Mavinic and F. A. Koch, *Can. J. Civil Eng*. 37, 1271 (2010).
[49] M. Weil, *Crystal. Res. Tech.* 43, 1286 (2008).
[50] A. A. Rouff and D. Maza, *Geochim. Cosmochim. Acta* 74, A887(2010).
[51] D. Paktunc and J. E. Dutrizac, *Can. Mineral*. 41, 905 (2003).
[52] K.S. Savage, D. K. Bird and P. A. O'Day, *Chem. Geol*. 215, 473 (2005).
[53] M. Delfini, M. Ferrini, A. Manni, P. Massacci and L. Piga, *Miner. Eng*. 16, 45 (2003).
[54] I. Alp, H. Deveci, Y. H. Süngün, E. Y. Yazici, M. Savaş and S. Demirçi, *Environ. Sci. Tech*. 43, 6939 (2009).
[55] A. Fernández-Martínez, G. Roman-Ross, G. J. Cuello, X. Turrillas, L. Charlet, M. R. Johnson and F. Bardelli, *Physica B* 385-386, 935 (2006).
[56] A. Fernández-Martínez, L. Charlet, G. J. Cuello, M. R. Johnson, G. Roman-Ross, F. Bardelli and X. Turrillas, *J. Phys. Chem*. A112, 5159 (2008).
[57] J. D. Rodríguez-Blanco, A. Jiménez and M. Prieto, *Crystal Growth Design* 7, 2756 (2007).
[58] J. D. Rodríguez, A. Jiménez, M. Prieto, L. Torre and S. García-Granda, *Amer. Mineral*. 93, 928 (2008).

[59] D. E. Garrett, *Borates: Handbook of Deposits, Processing, Properties, and Use*. Academic Press (1998).
[60] C. Helvaci and R.N. Alonso, *Turkish J. Earth Sci*. 9, 1 (2000).
[61] J. Lin, Y. Pan, N. Chen, M. Mao, R. Li and R. Feng, *Can. Mineral*. 49, 809 (2011).